Accelerated Sample-Accurate R-Peak Detectors Based on Visibility Graphs

Jonas Emrich, Taulant Koka, Sebastian Wirth, and Michael Muma

***Abstract*—The effective detection and accurate clinical diagnosis of cardiac conditions strongly relies on the correct localization of R-peaks in the electrocardiogram (ECG). Recently, demand for sample-accurate R-peak detection, which is essential to precisely reveal vital features, such as heart rate variability and pulse transit time, has increased. Therefore, we propose two novel sample-accurate visibility-graph-based R-peak detectors, the FastNVG and the FastWHVG detector. The visibility graph (VG) transformation maps a discrete signal into a graph by representing sampling locations as nodes and establishing edges between mutually visible samples. However, processing large-scale clinical ECG data urgently demands further acceleration of VG-based algorithms. The proposed methods reduce the required computation time by one order of magnitude and simultaneously decrease the required memory compared to a recently proposed VG-based R-Peak detector. Instead of transforming the entire ECG, the proposed acceleration benefits largely from building the VG based on a subset containing only the samples relevant to R-peak detection. Further acceleration is obtained by adopting the computationally efficient horizontal visibility graph, which has not yet been used for R-peak detection. Numerical experiments and benchmarks on multiple ECG databases demonstrate a significantly superior performance of the proposed VG-based methods compared to popular R-peak detectors.**

***Index Terms*—ECG, R-peak detection, Visibility graph**

I. Introduction

The precise detection of R-peaks in the electrocardiogram (ECG) is a crucial step for assessing cardiovascular health and is required in a variety of clinical and research settings. For example, estimates of heart rate variability (HRV) in pathological regions ($\leq 40\,\mathrm{ms}$ [1]) may be severely affected by even a few samples imprecision. A sample-accurate detection of R-peaks carries great significance for several applications, such as cuffless blood pressure estimation using the pulse transit time calculated from the peak positions in an ECG and a simultaneously recorded photoplethysmogram (PPG) [2] or HRV analysis [3]. While over the last five decades, a great quantity of detectors were developed (e.g., [4]–[11]), most of these detectors do not aim for a sample-accurate detection, which remains a difficult task. The difficulties arise, e.g., due to the presence of noise, motion artifacts [12], varying morphology of QRS complexes in different patients, health conditions and changing measurement settings.

Recently, Koka *et al.* proposed an R-peak detector that relies on a mapping of the ECG signal to a graph, which preserves important local features and captures nonstationary behavior [7]. Koka *et al.* made use of the so-called natural visibility graph (NVG) [13] and demonstrated its great potential for a sample-accurate detection of R-peaks. Despite this potential, the computation and storage of the NVGs for very large data sets is still expensive and further improvements are required.

In this work, we further explore the potential of visibility-graph-based R-peak detectors. In particular, two novel fast visibility-graph-based R-peak detectors are proposed that reduce the computation time by one order of magnitude compared to the detector by Koka *et al.*. The first detector (FastNVG) integrates an acceleration technique into the NVG, leading to a reduction of computation time of the graph building procedure and a reduction of the dimensionality of the adjacency matrix. The second detector (FastHVG) also builds upon this acceleration and further reduces the computation time and memory requirements by constructing a weighted version of the horizontal visibility graph (HVG). The HVG is a subgraph of the NVG that can be more efficiently computed due to its simpler geometry [14], [15], but its potential in R-Peak detection has, to the best of our knowledge, not been explored prior to this work. Using multiple benchmark ECG datasets, we show that the proposed methods yield a significant performance gain in terms of F_1-score and HRV estimation compared to popular R-peak detectors.

Organization: Section II introduces the methodology of the proposed algorithms and details the proposed detectors. Then, numerical results and benchmarks against established methods are provided in Section III, while Section IV draws a conclusion and gives an outlook to future work.

II. Methodology

This section presents the complete pipeline (Fig. 1) for the proposed accelerated R-peak detectors using visibility graphs. First, Section II-A describes two visibility graph transformations that represent the ECG signal as a graph. Subsequently, graph information is used to weight the ECG signal so as to emphasize R-peaks, as described in Section II-B. Finally, the R-peak positions are determined by thresholding the resulting signal, as outlined in Section II-C. Acceleration methods that reduce the computation time by an order of magnitude are presented in Section II-D. A python implementation will be made available on the authors github page.

A. Visibility Graph Transformations for R-peak Detection

The general idea underlying the visibility graph transformation [13] is to map a discrete-time series $x_n \in \mathbb{R}$ with

Taulant Koka (email: taulant.koka@tu-darmstadt.de) and Michael Muma (email: michael.muma@tu-darmstadt.de) are with the Robust Data Science Group at TU Darmstadt, Germany. Their work has been funded by the ERC Starting Grant ScReeningData under grant number 101042407.

The work of the first author has been funded by the LOEWE initiative (Hesse, Germany) within the emergenCITY center.

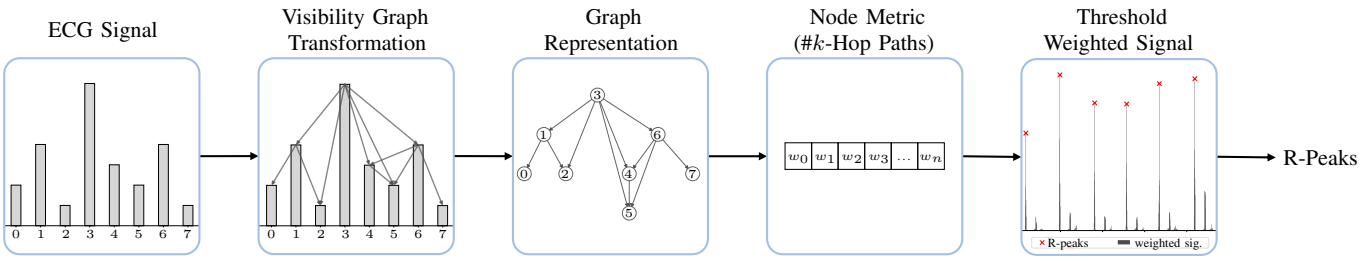

Fig. 1: Illustration of the pipeline for the visibility-graph-based R-peak detector: First, the time series is mapped into a graph representation using the NVG transformation, as depicted in the second block. Subsequently, a node metric is calculated in the graph domain, to weight the original signal, emphasizing R-peak positions, which are then extracted by a thresholding procedure.

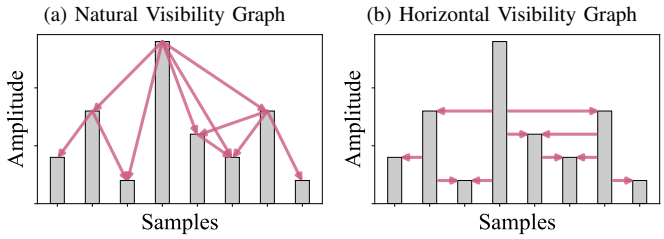

Fig. 2: Visualization of the visibility criterion used for creating directed edges (top-to-bottom) in the NVG on the left (2a) and HVG on the right (2b).

associated locations $t_n \in \mathbb{R},\ n = 0, \dots, N-1$ to a graph $\mathcal{G} = (\mathcal{V}, \mathcal{E})$, where $\mathcal{V}$ is a set of vertices and $\mathcal{E}$ is a set of edges. For every sampling location t_n, a corresponding vertex $v_n \in \mathcal{V}$ is created and edges between vertices are established according to a visibility criterion determined by the graph transformation. While numerous visibility graph transformations employing a range of criteria for edge generation have been proposed in the literature [14]–[17], this work focuses on the NVG and the computationally efficient HVG, which is a subgraph of the NVG [13], [14]. The graphs are generated by adding edges $\varepsilon_{a,b}$ to $\mathcal{E}$, whenever the associated points $(t_a, x_a), (t_b, x_b)$ satisfy some relation for all intermediate points (t_c, x_c) with $t_a < t_c < t_b$. In particular, the NVG is constructed by employing the criterion

$$x_c < x_b + (x_a - x_b) \cdot \frac{x_b - x_a}{t_b - t_a}, \tag{1}$$

while the HVG is obtained from

$$x_c < \min\{x_a, x_b\}. \tag{2}$$

The intuition behind (1) and (2) is that for the NVG (Fig. 2a) an edge is formed when a straight line of sight exists between two points, whereas the HVG (Fig. 2b) requires the line of sight to be horizontal.

In this work, we utilize directed versions of the NVG and HVG transformations that establish directed edges from larger to smaller points (top-to-bottom). In this case, the maximum value of the time series is represented as the source node in the graph and local minima are sinks resulting in a directed acyclic graph (DAG) [7]. As we will see later, the chosen visibility criteria lead to a sparse graph that represents R-peaks as nodes of high connectivity.

Unfortunately, a direct application of the HVG has proven to be unsuitable for R-peak detection, i.e., it does not lead to reliable R-peak detections. However, we conjecture that the incorporation of additional edge weight information that is not captured by the simple (but computationally efficient) graph generation process may benefit the R-peak detection capacity of the HVG. The weighted graph is then defined as a triple $\mathcal{G}_w = (\mathcal{V}, \mathcal{E}, \omega)$, where $\omega : \mathcal{E} \to \mathcal{W}$ maps each edge to a set of weights $\mathcal{W}$. In this work, extensive numerical experiments have been conducted to benchmark the influence of various edge weights on the performance in terms of R-peak detection. Considered weights include the Euclidean distance, the horizontal and vertical distance, the slope, and the angle, each computed with respect to the line segment between the two points defining the edge. Empirical observations (which are omitted for the sake of brevity) suggest that the weighted edges provide a significant benefit for the HVG, in the application of R-peak detection. Specifically, the absolute slope

$$\omega(\varepsilon_{a,b}) = \left| \frac{x_a - x_b}{t_a - t_b} \right|, \tag{3}$$

yields a larger gain compared to other edge weights and is therefore utilized in the HVG transformation in the following, resulting in the weighted horizontal visibility graph (WHVG).

B. k-Hop Paths: A Node Property to Emphasize R-Peaks

As demonstrated in [7], the number of k-hop paths, in short, the *k-hop centrality*, is a suitable node property to emphasize R-peaks. It is defined as the number of paths of length k that start at a given node. When $k = 1$, the metric represents the outdegree of the node, which is the sum of the weights of all outgoing edges. For a DAG, the k-hop centrality $\boldsymbol{c}$ can be computed as

$$\boldsymbol{c} = \mathbf{A}^k \mathbf{1}, \tag{4}$$

where $\mathbf{A}$ is the adjacency matrix of the graph $\mathcal{G}$ and $\mathbf{1} = (1, \dots, 1)^\top$ is the all-ones vector of length N. Note that for a weighted graph, such as the WHVG, (4) yields a weighted k-hop centrality. To prevent the values in (4) from becoming impractically large, the normalized centrality $\bar{\boldsymbol{c}}$ is adopted and calculated iteratively as follows:

$$\bar{\boldsymbol{c}}_{i+1} = \frac{\mathbf{A}\bar{\boldsymbol{c}}_i}{\|\mathbf{A}\bar{\boldsymbol{c}}_i\|_2}, i \in [0, k]. \tag{5}$$

In the first iteration, the normalized centrality is initialized as $\bar{\boldsymbol{c}}_0 = \mathbf{1}/N$, and (5) is iterated k times. Note, that for an undirected graph, (5) converges to the eigenvector centrality [18]. For a DAG, however, the entries of $\bar{\boldsymbol{c}}_i$ in (5) converge to zero if k exceeds the length of the longest path starting at the respective node. Therefore, the iterative computation of the weight vector is stopped when $\bar{\boldsymbol{c}}_i$ reaches a pre-defined sparsity level β, i.e., when $\|\bar{\boldsymbol{c}}_i\|_0/N \leq \beta$. Here, $\|\bar{\boldsymbol{c}}_i\|_0$ denotes the number of nonzero elements in $\bar{\boldsymbol{c}}_i$. See Section III-A and Fig. 3 for the choice of β. In summary, as the sparsity of the weight vector increases with increasing path length k, highly connected nodes with long path lengths, such as R-peaks in an ECG signal, are emphasized (see Fig. 1).

C. Threshold

The R-peak positions in the weighted ECG signal can be extracted by applying a thresholding method, such as the one developed by Pan and Tompkins [4], which has been applied in many R-peak detectors, e.g., [5], [7], [19]. We adapted a commonly used Python implementation [20] and made the following minor modifications: (i) The signal and noise thresholds were initialized as described in the original paper by Pan and Tompkins [4]. (ii) Peak candidates that occur in close proximity to previously detected R-peaks (i.e., those with a distance smaller than the minimum peak distance of 300 ms) are compared, and only the candidate with the highest weighted signal value is considered, while the other candidates are discarded. (iii) The searchback procedure was modified to take into account not only previous peak candidates, but also any samples above the noise threshold that are further than the minimum peak distance away from adjacent peaks.

D. Acceleration

In clinical practice, long-term ECG monitoring and data collection in biobanks may lead to extensive amounts of collected data. Thus, a fast runtime of R-peak detectors is crucial. For this reason, acceleration techniques that reduce the computation time compared to [7] by one order of magnitude (see Section III) are proposed below.

As shown in [7], the time complexity of visibility-graph-based R-peak detectors that employ a segmentation is linear in the number of segments. We therefore propose a data reduction technique to accelerate the computation of individual segments by considering only a subset of samples for graph construction. More precisely, we only consider the set of local maxima that is greater than the median of the segment. Such an acceleration is reasonable since the R-peaks are, with high probability, elements of the subset. By contrast, samples with small amplitudes are neglected. As a consequence, the dimensions of the adjacency matrix $\mathbf{A}$ and the weight vector $\bar{\boldsymbol{c}}$ are significantly reduced. This leads to a faster graph construction in (1) and (2) and a faster computation of the matrix-vector product in (5).

Further reduction of the computation and memory requirements is obtained by adopting the HVG for R-peak detection. As a subgraph of the NVG, the HVG requires less memory and computation steps. Additionally, a major advantage of the HVG compared to the NVG is that fast implementations, such as [21] and [22], exist, which can be calculated with a worst-case time complexity of linear time $\mathcal{O}(n)$. In contrast, for the NVG, even efficient methods, such as the binary search tree [23] or the divide-and-conquer algorithm [24], have an average time complexity of $\mathcal{O}(n \log n)$, which degrades to $\mathcal{O}(n^2)$ in the worst case. Accelerating the NVG and WHVG detectors with the proposed methodology yields the proposed FastNVG and FastWHVG detectors, respectively.

III. Simulations

This section is dedicated to the evaluation of the proposed R-peak detectors. The experiments investigate the selection of the sparsity parameter β (III-A), examine the introduced acceleration (III-B) and compare the detection accuracy, by evaluating it within a tolerance window of zero and five samples (III-C). The evaluation is conducted on real data including a dataset from the Glasgow University Database (GUDB) [25], which provides highly accurate annotations, allowing for sample-accurate benchmarking, as well as the well-established MIT-BIH Arrhythmia Database (MITDB) [26], [27].

A. Sparsity Parameter Selection

Empirical experiments in [7] based on the GUDB suggest that a sparsity parameter of $\beta = 0.55$ (i.e., 55% of the entries of $\bar{\boldsymbol{c}}$ are nonzero) provides best results for the NVG detector in the application of R-peak detection, while the performance remains stable over a broad sparsity region around this value. Similar observations were made for the FastNVG detector, where the sparsity level is computed with respect to the dimension of the reduced data vector.

We also conducted numerical benchmarks on the GUDB to determine the optimal beta for the FastWHVG detector. To this end, we look at two performance measures. Firstly, the F_1-score, which considers both precision and recall and is given by

$$\mathrm{F}_1 = \frac{2\mathrm{TP}}{2\mathrm{TP} + \mathrm{FP} + \mathrm{FN}}, \tag{6}$$

where TP, FP, FN denote the number of correct, false and missed R-peak detections, respectively; and secondly, the

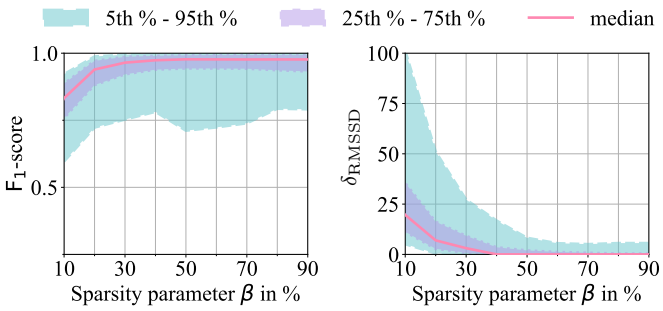

Fig. 3: Sample-accurate evaluation of the FastWHVG for several nonzero weight elements. To make a compromise between F_1-score and relative RMSSD error δ_{RMSSD}, a sparsity parameter value of $\beta = 85\%$ is seletced.

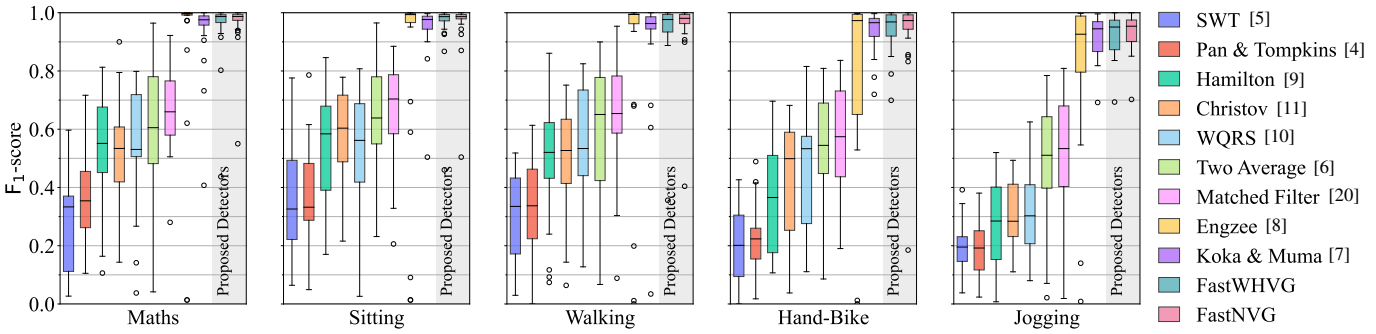

Fig. 4: Evaluation of the proposed detectors against several established R-peak detection methods on the GUDB [25] using a zero tolerance window.

relative error of the root mean square of successive differences (RMSSD). The RMSSD is given by

$$\mathrm{RMSSD} = \sqrt{\frac{1}{M-1}\sum_{m=1}^{M}(\mathrm{RR}_{m+1} - \mathrm{RR}_m)^2}, \qquad (7)$$

where RR_m is the mth interval between two successive R-peaks and M is the number of RR intervals. The relative error of the estimate $\widehat{\mathrm{RMSSD}}$, which we denote as δ_{RMSSD}, is computed as

$$\delta_{\mathrm{RMSSD}} = \left| \frac{\widehat{\mathrm{RMSSD}} - \mathrm{RMSSD}}{\mathrm{RMSSD}} \right|. \qquad (8)$$

Fig. 3 provides an empirical evaluation of the F_1-score and δ_{RMSSD} as functions of the sparsity parameter β, where an optimal value of β is one, which minimizes the average δ_{RMSSD} and simultaneously maximizes the average F_1-score, while maintaining low variance. For the FastWHVG, it can be observed that the performance remains stable over a broad interval, with a slight drop in the 5th percentile of the F_1-score for $45\% \leq \beta \leq 75\%$. Therefore, a target level of $\beta = 85\%$ is utilized for the FastWHVG in all our experiments.

B. Runtime

In order to evaluate the introduced acceleration, the proposed algorithms are benchmarked on the GUDB against [7] in terms of their relative runtime compared to the median runtime of Koka *et al.*, as depicted in Fig. 5. It is shown, that both of the proposed accelerated detectors, i.e., utilizing the NVG and WHVG, introduce a significant runtime improvement of up to 90% in comparison to [7]. The median runtimes compared to [7] are 11.65% for the FastNVG and 9.78% for the FastwWHVG, respectively. Since all variants use the same segmentation method, i.e., fixed sized segments for computation, the observed acceleration is solely attributed to a faster computation.

C. Detection Accuracy

To evaluate the detection accuracy, the proposed methods are compared against several established R-peak detectors, i.e., Stationary Wavelet Transform (SWT) [5], WQRS [10], Two Moving Average [6], Matched Filter [20], as well as

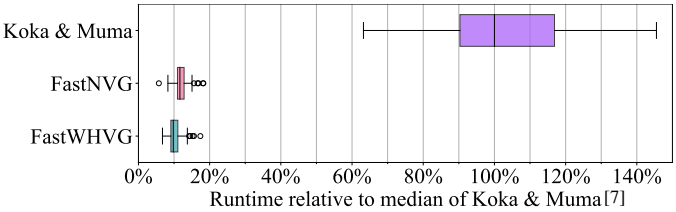

Fig. 5: Runtime comparison between the proposed detectors and the detector of Koka et al. on the GUDB. The runtime is shown in relation to the median runtime of the detector in [7].

the detectors by Pan & Tompkins [4], Hamilton [9], Christov [11], Engelse & Zeelenberg [8] and Koka & Muma [7]. Since most of the detectors proposed in the literature introduce a time delay due to the use of causal filters, the median time difference between the detected R-peak positions and the annotated R-peaks in the ECG signal was subtracted for each recording.

1) Performance on GUDB: The GUDB provides sample accurately annotated ECG recordings of 25 subjects performing five different activities, ranging from solving math problems to jogging. For a sample-accurate comparison, the ECG data recorded by a chest strap was evaluated and the resulting F_1-scores are shown in Fig. 4. In all cases, the methods by [8] and [7] as well as the proposed ones perform best. However, in the last two experiments, where signals are more noisy due to movement artifacts, the F_1-score of Engzee degrades, while the visibility-graph-based detectors, i.e., [7] and the proposed FastHVG and FastNVG detectors, retain a comparatively high accuracy. In addition, it can be observed that the FastNVG performs slightly better than the FastWHVG.

2) Performance on MITDB: The evaluation on the MITDB, assessing the F_1-score and δ_{RMSSD}, was performed using the signals from Lead I of the 48 recordings, with five sample tolerance to account for imprecision in the annotated R-peak locations (Fig. 6). Again, the proposed detectors are the best performing methods, i.e., they yield the highest F_1-scores of all considered detectors. Furthermore, the visibility graph based methods show a low δ_{RMSSD}, whereas [8] exhibits a significantly larger error, although it reached high F_1-scores on the GUDB. Note that imperfections in the annotations may lead to a biased RMSSD error, i.e., even a perfect R-peak

estimator cannot reach a zero error.

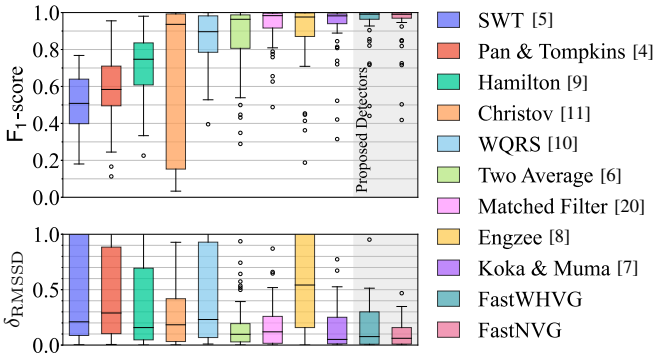

Fig. 6: Comparison of the F_1-score and δ_{RMSSD} (as in (8)) for the evaluated methods on the MITDB [26] using a tolerance window of five samples.

IV. Conclusion

In this work, the FastNVG and the FastWHVG detectors, which are based on the visibility graph transformation for time series, were proposed. The introduced acceleration method reduces the computation time of the proposed methods by an order of magnitude compared to [7], while also reducing the required memory. Numerical evaluations evidence the applicability of the proposed methods in sample-accurate R-peak detection, which was demonstrated on a high-precision ECG database. Moreover, the proposed detectors performed excellently on multiple ECG datasets and have shown a significant gain in performance compared to established methods. Exploring and further developing the proposed methods for related biomedical signals, such as PPG signals [28], is of great interest and will thus be the subject of future work.

References

[1] N. Singh, K. J. Moneghetti, J. W. Christle, D. Hadley, V. Froelicher, and D. Plews, "Heart rate variability: An old metric with new meaning in the era of using mhealth technologies for health and exercise training guidance. part two: Prognosis and training," *Arrhythmia & Electrophysiology Review 2018;7(4):247–55.*, 2018.

[2] Y. Choi, Q. Zhang, and S. Ko, "Noninvasive cuffless blood pressure estimation using pulse transit time and Hilbert–Huang transform," *Computers & Electrical Engineering*, vol. 39, no. 1, pp. 103–111, 2013, special issue on Recent Advanced Technologies and Theories for Grid and Cloud Computing and Bio-engineering.

[3] D. P. Williams, J. Koenig, L. Carnevali, A. Sgoifo, M. N. Jarczok, E. M. Sternberg, and J. F. Thayer, "Heart rate variability and inflammation: A meta-analysis of human studies," *Brain, Behavior, and Immunity*, vol. 80, pp. 219–226, 2019.

[4] J. Pan and W. J. Tompkins, "A Real-Time QRS Detection Algorithm," *IEEE Transactions on Biomedical Engineering*, vol. BME-32, no. 3, pp. 230–236, 1985.

[5] V. Kalidas and L. Tamil, "Real-time QRS detector using Stationary Wavelet Transform for Automated ECG Analysis," in *2017 IEEE 17th International Conference on Bioinformatics and Bioengineering (BIBE)*, 2017, pp. 457–461.

[6] M. Elgendi, M. Jonkman, and F. De Boer, "Frequency Bands Effects on QRS Detection." in *BIOSIGNALS 2010 - Proceedings of the 3rd International Conference on Bio-inpsired Systems and Signal Processing*, Jan. 2010, pp. 428–431.

[7] T. Koka and M. Muma, "Fast and Sample Accurate R-Peak Detection for Noisy ECG Using Visibility Graphs," in *2022 44th Annual International Conference of the IEEE Engineering in Medicine & Biology Society (EMBC)*, 2022, pp. 121–126.

[8] W. Engelse and C. Zeelenberg, "A single scan algorithm for QRS detection and feature extraction," *IEEE Computers in Cardiology*, vol. 6, no. 1, pp. 37–42, 1979.

[9] P. Hamilton, "Open source ECG analysis," in *Computers in Cardiology*, 2002, pp. 101–104.

[10] W. Zong, G. Moody, and D. Jiang, "A robust open-source algorithm to detect onset and duration of QRS complexes," in *Computers in Cardiology*, 2003, pp. 737–740.

[11] I. I. Christov, "Real time electrocardiogram QRS detection using combined adaptive threshold," *Biomedical engineering online*, vol. 3, no. 1, pp. 1–9, 2004.

[12] F. Strasser, M. Muma, and A. M. Zoubir, "Motion artifact removal in ecg signals using multi-resolution thresholding," in *2012 Proceedings of the 20th European Signal Processing Conference (EUSIPCO)*, 2012, pp. 899–903.

[13] L. Lacasa, B. Luque, F. Ballesteros, J. Luque, and J. C. Nuño, "From time series to complex networks: The visibility graph," *Proceedings of the National Academy of Sciences*, vol. 105, no. 13, pp. 4972–4975, Apr. 2008.

[14] B. Luque, L. Lacasa, F. Ballesteros, and J. Luque, "Horizontal visibility graphs: Exact results for random time series," *Physical Review E*, 2010.

[15] L. Lacasa, "Horizontal visibility graphs from integer sequences," *Journal of Physics A: Mathematical and Theoretical*, vol. 49, no. 35, p. 35LT01, Jul. 2016.

[16] M. Wang, A. L. M. Vilela, R. Du, L. Zhao, G. Dong, L. Tian, and H. E. Stanley, "Exact results of the limited penetrable horizontal visibility graph associated to random time series and its application," *Scientific Reports*, vol. 8, no. 1, p. 5130, Dec. 2018.

[17] Q. Xuan, J. Zhou, K. Qiu, D. Xu, S. Zheng, and X. Yang, "Clpvg: Circular limited penetrable visibility graph as a new network model for time series," *Chaos: An Interdisciplinary Journal of Nonlinear Science*, vol. 32, no. 1, p. 013130, 2022.

[18] G. Russo, V. Nicosia, and V. Latora, "Centrality Measures," in *Complex Networks: Principles, Methods and Applications*. Cambridge: Cambridge University Press, 2017, pp. 31-68.

[19] B. Porr and L. Howell, "R-peak detector stress test with a new noisy ECG database reveals significant performance differences amongst popular detectors," *bioRxiv*, 2019.

[20] B. Porr, L. Howell, I. Stournaras, and Y. Nir, "Popular ECG R peak detectors written in python," Jul. 2022.

[21] G. Zhu, Y. Li, and P. Wen, "Epileptic seizure detection in EEGs signals using a fast weighted horizontal visibility algorithm," *Computer methods and programs in biomedicine*, vol. 115 2, pp. 64–75, 2014.

[22] C. Stephen, "A Scalable Linear-Time Algorithm for Horizontal Visibility Graph Construction Over Long Sequences," in *2021 IEEE International Conference on Big Data (Big Data)*, 2021, pp. 40–50.

[23] D. Fano Yela, F. Thalmann, V. Nicosia, D. Stowell, and M. Sandler, "Online visibility graphs: Encoding visibility in a binary search tree," *Physical Review Research*, vol. 2, no. 2, p. 023069, Apr. 2020.

[24] X. Lan, H. Mo, S. Chen, Q. Liu, and Y. Deng, "Fast transformation from time series to visibility graphs," *Chaos: An Interdisciplinary Journal of Nonlinear Science*, vol. 25, no. 8, p. 083105, 2015.

[25] L. Howell and B. Porr, "High precision ECG Database with annotated R peaks, recorded and filmed under realistic conditions," Dec. 2018, publisher: University of Glasgow. [Online]. Available: https://researchdata.gla.ac.uk/716/

[26] G. Moody and R. Mark, "The impact of the MIT-BIH Arrhythmia Database," *IEEE Engineering in Medicine and Biology Magazine*, vol. 20, no. 3, pp. 45–50, 2001.

[27] A. L. Goldberger, L. A. N. Amaral, L. Glass, J. M. Hausdorff, P. C. Ivanov, R. G. Mark, J. E. Mietus, G. B. Moody, C.-K. Peng, and H. E. Stanley, "Physiobank, physiotoolkit, and physionet: components of a new research resource for complex physiologic signals." *Circulation*, vol. 101 23, pp. E215–20, 2000.

[28] T. Schäck, C. Sledz, M. Muma, and A. M. Zoubir, "A new method for heart rate monitoring during physical exercise using photoplethysmographic signals," in *2015 23rd European Signal Processing Conference (EUSIPCO)*, 2015, pp. 2666–2670.